EINDHOVEN UNIVERSITY OF TECHNOLOGY

Atomic layer deposition of HfO2 using HfCp(NMe2)3 and O2 plasma

Citation for published version (APA):
Sharma, A., Longo, V., Verheijen, M. A., Bol, A. A., & Kessels, W. M. M. (2017). Atomic layer deposition of HfO2 using HfCp(NMe2)3 and O2 plasma. *Journal of Vacuum Science and Technology A*, *35*(1), Article 01B130. https://doi.org/10.1116/1.4972210

DOI:
10.1116/1.4972210

Document status and date:
Published: 01/01/2017

Document Version:
Publisher's PDF, also known as Version of Record (includes final page, issue and volume numbers)

Please check the document version of this publication:

• A submitted manuscript is the version of the article upon submission and before peer-review. There can be important differences between the submitted version and the official published version of record. People interested in the research are advised to contact the author for the final version of the publication, or visit the DOI to the publisher's website.
• The final author version and the galley proof are versions of the publication after peer review.
• The final published version features the final layout of the paper including the volume, issue and page numbers.

Link to publication

General rights
Copyright and moral rights for the publications made accessible in the public portal are retained by the authors and/or other copyright owners and it is a condition of accessing publications that users recognise and abide by the legal requirements associated with these rights.

• Users may download and print one copy of any publication from the public portal for the purpose of private study or research.
• You may not further distribute the material or use it for any profit-making activity or commercial gain
• You may freely distribute the URL identifying the publication in the public portal.

If the publication is distributed under the terms of Article 25fa of the Dutch Copyright Act, indicated by the "Taverne" license above, please follow below link for the End User Agreement:

www.tue.nl/taverne

Take down policy
If you believe that this document breaches copyright please contact us at:

openaccess@tue.nl

providing details and we will investigate your claim.

Download date: 16. Nov. 2023

.

Atomic layer deposition of HfO_2 using $HfCp(NMe_2)_3$ and O_2 plasma

Akhil SharmaValentino LongoMarcel A. VerheijenAgeeth A. Bol and W. M. M. (Erwin) Kessels

Citation: J. Vac. Sci. Technol. A **35**, 01B130 (2017); doi: 10.1116/1.4972210
View online: http://dx.doi.org/10.1116/1.4972210
View Table of Contents: http://avs.scitation.org/toc/jva/35/1
Published by the American Vacuum Society

Articles you may be interested in

Plasma-assisted atomic layer deposition of HfNx: Tailoring the film properties by the plasma gas composition
J. Vac. Sci. Technol. A **35**, 01B129 (2016); 10.1116/1.4972208

Low-temperature-atomic-layer-deposition of SiO2 using various organic precursors
J. Vac. Sci. Technol. A **35**, 01B131 (2016); 10.1116/1.4972211

Plasma-assisted atomic layer deposition of conformal Pt films in high aspect ratio trenches
J. Vac. Sci. Technol. A **146**, 052818 (2016); 10.1063/1.4972120

Tris(dimethylamido)aluminum(III): An overlooked atomic layer deposition precursor
J. Vac. Sci. Technol. A **35**, 01B128 (2016); 10.1116/1.4972469

RIGHTSLINK

CrossMark
click for updates

Atomic layer deposition of HfO_2 using $HfCp(NMe_2)_3$ and O_2 plasma

Akhil Sharma[a)]
Department of Applied Physics, Eindhoven University of Technology, P.O. Box 513, 5600 MB Eindhoven, The Netherlands

Valentino Longo[a)]
ams AG, Tobelbader Strasse 30, A-8141 Premstaetten, Austria

Marcel A. Verheijen
Department of Applied Physics, Eindhoven University of Technology, P.O. Box 513, 5600 MB Eindhoven, The Netherlands and Philips Innovation Services, High Tech Campus 4, 5656 AE Eindhoven, The Netherlands

Ageeth A. Bol and W. M. M. (Erwin) Kessels[b)]
Department of Applied Physics, Eindhoven University of Technology, P.O. Box 513, 5600 MB Eindhoven, The Netherlands

(Received 23 September 2016; accepted 29 November 2016; published 20 December 2016)

HfO_2 thin films were prepared by plasma-enhanced atomic layer deposition using a cyclopentadienyl-alkylamido precursor [$HfCp(NMe_2)_3$, HyALD^{TM}] and an O_2 plasma over a temperature range of 150–400 °C at a growth per cycle around 1.1 Å/cycle. The high purity of the films was demonstrated by x-ray photoelectron spectroscopy and elastic recoil detection analyses which revealed that by increasing the deposition temperature from 200 to 400 °C, the atomic concentrations of residual carbon and hydrogen reduced from 1.0 to <0.5 at. % and 3.4 to 0.8 at. %, respectively. Moreover, Rutherford backscattering spectroscopy studies showed an improvement in stoichiometry of HfO_2 thin films with the increase in deposition temperature, resulting in Hf/O ratio close to ~0.5 at 400 °C. Furthermore, grazing incidence x-ray diffraction measurements detected a transition from amorphous at the deposition temperature of 300 °C to fully polycrystalline films at 400 °C, consisting of a mixture of monoclinic, tetragonal, and cubic phases. Finally, the surface morphology and conformality of HfO_2 thin films studied by atomic force microscopy and transmission electron microscopy are also reported. © *2016 American Vacuum Society*.
[http://dx.doi.org/10.1116/1.4972210]

I. INTRODUCTION

Atomic layer deposition (ALD) of high-k dielectric materials has been a subject of intensive research over the past years. Among such high-k oxides, hafnium oxide (HfO_2) has been endorsed largely for the application of high-k gate oxide in complementary metal oxide semiconductor devices owing to its high permittivity, fairly large band gap, and ability to form a thermodynamically stable interface with Si.[1–5] The application of HfO_2 as a gate oxide material is not only limited to conventional Si based devices but also extending its horizons in novel nanomaterials based devices. For instance, Radisavljevic *et al.* have recently shown that by implementing HfO_2 as gate oxide for a field effect transistor device based on an emerging 2D-nanomaterial, molybdenum disulphide (MoS_2), the mobility could be drastically boosted owing to the suppression of coulombic scattering via dielectric screening.[6] Furthermore, most recently, the application of a gate stack based on HfO_2/Al_2O_3/III-V($In_{0.53}Ga_{0.47}As$) for metal-oxide-semiconductor capacitor devices has been demonstrated by Djara *et al.*[7] These devices have a HfO_2/Al_2O_3 stack as gate oxide deposited by plasma enhanced ALD (PEALD) and show a low interface trap density (D_{it}). Additionally, HfO_2 also finds applications as a protective coating for microelectromechanical systems and as insulator for organic devices such as organic light emitting diode and organic field effect transistors.[8–10]

ALD has been the method of choice for depositing thin films of HfO_2. The self-saturating nature of the ALD process enables atomic level control over thickness and uniformity and this makes ALD ideal for preparing ultrathin HfO_2 thin films. In particular, the much needed conformality over high aspect ratio structures in combination with the excellent uniformity over large surface areas and the pin-hole free nature of the ALD produced thin films makes ALD a befitting deposition process.[4,11]

In ALD, the choice of precursor has a large effect on the quality and properties of the deposited thin films. This leads to a continuous effort in precursor synthesis aiming at improving temperature stability and/or reducing impurity concentrations in the resulting film depending on the final application. In literature, a number of Hf precursors have been implemented for HfO_2 ALD processes. The established ALD processes leave a room for improvement in terms of extension of operating conditions. In this contribution, we have investigated a novel precursor, $HfCp(NMe_2)_3$, in combination with O_2 plasma which has yielded into a viable HfO_2 ALD process with a constant growth rate over the widest possible range of operating conditions such that it is suited for a multitude of applications. The details of the process investigated will be discussed in this paper. However, it is useful to systematically look at established ALD processes as listed in Table I, where a brief overview of efforts

[a)]A. Sharma and V. Longo contributed equally to this work.
[b)]Electronic mail: w.m.m.kessels@tue.nl

 © 2016 American Vacuum Society

RIGHTSLINK

TABLE I. Overview of selected ALD processes reported in the literature for HfO_2 thin film with various Hf precursors. Me = CH_3, Et = C_2H_5, Cp = C_5H_5.

Precursor group	Hafnium precursor/oxygen source	Growth temperature range (°C)	Substrate(s) used	Growth per cycle (Å)	References
Halides	$HfCl_4/H_2O$	500	Glass	0.5	12
	$HfI_4/HfCl_4/H_2O$	300	Si[a]	0.47–0.62	13
Alkylamides	$Hf[NMeEt]_4/H_2O$	150–325	Glass, SiO_2/Si	0.9–1.5	17
	$Hf(NEt_2)_4/H_2O$	50–500	Si[a]	0.9	18
	$Hf[NMeEt]_4/O_3$	120–300	SiO_2/Si	0.8–1.1	19
	$Hf[NMe_2]_4/H_2O$	300	Si[a]	0.78	3
	$Hf[NMeEt]_4/O_2$ plasma	230–350	Si[a]	1.0	20
Cyclo-pentadienyls	Cp_2HfMe_2/H_2O	300–500	SiO_2/Si	0.42	21
	$(CpMe)_2Hf(OMe)Me/O_3$	350–500	Si[a], SiO_2/Si	0.5	22
Alkylamides + Cyclo-pentadienyls	$CpHf(NMe_2)_3/H_2O$	305–410	SiO_2/Si	0.23–0.36	23
	$CpHf(NMe_2)_3/O_3$	250–400	SiO_2/Si	0.7–0.8	24
	$CpHf(NMe_2)_3/O_2$ plasma	150–400	Si[a], SiO_2/Si	1.1	This study

[a]HF last treated.

reported in literature focusing on detailed investigation of the ALD processes by using four different precursor groups for HfO_2 thin films is given. The most frequently used precursor for HfO_2 ALD is $HfCl_4$ which is combined with H_2O or O_3 as oxygen source.[2,12–15] However, the limitations associated with this precursor, such as corrosive byproducts and poor nucleation on H-terminated Si at high temperatures (≥300 °C), make this precursor unfavorable for some specific applications like dynamic random-access memories and therefore have led for a search for alternative precursor chemistries.[2,15,16]

One of such a widely applied alternative precursor group for HfO_2 ALD is alkylamide comprising metal–nitrogen bonds, namely $Hf(NEtMe)_4$ (TEMAH), $Hf(NEt_2)_4$, and $Hf(NMe_2)_4$ (Et = C_2H_5, Me = CH_3).[3,17–20] These alkylamide type precursors possess a high volatility and reactivity and yield a high growth per cycle (GPC) in combination with H_2O or O_3 as coreactants.[17] However, they suffer from a limited thermal stability which can lead to a parasitic CVD component and might result into high impurity concentrations and poor film uniformity.[25] In addition, Kukli *et al.* have demonstrated that the HfO_2 ALD process using TEMAH in combination with H_2O as oxygen source leads to an increment in GPC from 0.9 Å/cycle at 250 °C to 1.5 Å/cycle at 325 °C, indicating the decomposition of the precursor at temperatures ≥300 °C.[17]

To overcome this, an ALD process using the cyclopentadienyl (Cp = C_5H_5) precursor type was investigated. A higher thermal stability was achieved and ALD saturation was realized at a relative high substrate temperature of 400 °C.[22] However, a lower GPC of ∼0.5 Å/cycle was obtained when using Cp-precursors like $(CpMe)_2HfMe_2$ and $(CpMe)_2Hf(OMe)Me$ as compared to the alkylamides (∼0.9 Å/cycle).[19]

With the aim of combining the benefits of both precursor types, precursors comprising both cyclopentadienyl and alkylamide type ligands have been investigated.[23,24] A high thermal stability and high GPC attributed to cyclopentadienyl ligands and alkylamide ligands, respectively, have been demonstrated for both Hf and Zr based ALD processes.[23,24,26] For ZrO_2, this combined merit of high thermal stability and high growth per cycle has been manifested by using a chemically analogous precursor, i.e., $CpZr(NMe_2)_3$ in combination with H_2O, where a growth per cycle of 0.8–1 Å/cycle in the temperature range of 120–350 °C was obtained.[26] However, a similar Hf precursor containing mixed cyclopentadienyl and alkylamide ligands, i.e., $HfCp(NMe_2)_3$ when applied in combination with H_2O yielded a growth per cycle of only 0.23–0.36 Å/cycle in the temperature range of 305–375 °C.[23] Furthermore, Niinistö *et al.* have shown that the use of a stronger oxidant like O_3 in combination with $HfCp(NMe_2)_3$ yields a higher growth per cycle (0.75 Å/cycle) in the temperature range of 250–350 °C.[24] The higher growth in the latter case might be attributed to the high reactivity of O_3 at a relatively low temperature resulting in the efficient removal of the bulky Cp ligands.[24] However, both with H_2O or O_3 as oxidizing agents, depositions have not been reported below 250 °C, which might be necessary for HfO_2 film deposition on temperature-sensitive substrates, in particular, for organic device applications and flexible electronics based on novel nanomaterials.[10,27] In this context, another alternative is to employ a plasma enhanced ALD process (i.e., O_2 plasma as oxygen source) in combination with the same Hf precursor [$HfCp(NMe_2)_3$] for growth of HfO_2 thin films. It is well known that the use of plasma chemistry offers potential advantages like improved material properties, feasibility of lower deposition temperatures, and increased flexibility in process conditions.[28]

In the present study, we report the $HfCp(NMe_2)_3$ in combination with an O_2 plasma process which yields a fairly high growth per cycle over a wide ALD temperature window (150–400 °C) while retaining the high material properties. A detailed characterization of the HfO_2 PEALD process has been carried out. The dependence of film growth rate on various parameters like growth temperature and duration of dose during the plasma enhanced ALD process has been studied. Furthermore, an elaborated material characterization elucidating the film structure and composition depending on growth temperature has been performed. Finally, in order to assert the potential of ALD to deposit conformally on 3D structures, the film conformality over high aspect ratio structures has also been demonstrated.

RIGHTSLINK

II. EXPERIMENT

A. Film deposition

The HfO_2 thin films were deposited in an Oxford Instruments FlexAL™ ALD reactor on 100–200 mm Si wafers either with a native oxide layer or H-terminated as created by a hydrofluoric acid (HF)-last process (1% HF). The Hf precursor employed was $HfCp(NMe_2)_3$, HyALD™, obtained from AirLiquide. The precursor was stored in a stainless steel canister and heated to 60 °C. At this temperature, the vapor pressure of the HyALD precursor is approximately 100 mTorr.[29] For the precursor delivery to the deposition chamber a 100 sccm Ar (>99.999% purity) bubbling flow was employed. An Ar purge step with 100 sccm of Ar flow was applied after the precursor and plasma exposure steps. To avoid condensation of the precursor, the delivery lines were kept at 90 °C while the reactor walls were heated to 120 °C. As the oxidizing agent, an O_2 (>99.999% purity) plasma generated in an inductively coupled plasma source was used. The reactor pressure during the plasma step was 15 mTorr. The plasma power used was 400 W. The substrate stage was heated to temperatures in the range of 150–400 °C during the deposition processes. It is worth mentioning that there was a ~20%–25% difference between the set temperature value and the actual substrate temperature for the reactor employed in this work.

B. Film analysis

The thickness and the optical properties of the HfO_2 thin films were measured by spectroscopic ellipsometry (SE). *Ex situ* measurements (J.A. Woollam M2000D) were performed to determine the final thickness and the dielectric function in the 1.25–6.5 eV spectral range. The film thickness evolution during deposition was monitored by *in situ* measurements (J.A. Woollam M2000F, 1.25–5 eV).

To determine the elemental composition and the density of the films Rutherford backscattering spectroscopy (RBS) was used. Furthermore, elastic recoil detection (ERD) was employed to determine the hydrogen content in the films. Both RBS and ERD were performed using a 2 MeV $^4He^+$ ion flux (Acctec BV, The Netherlands). X-ray photoelectron spectroscopy (XPS) was also performed using a Thermo Scientific K-alpha spectrometer using monochromatic Al Kα x-ray radiation ($h\nu = 1486.6$ eV). XPS was used to quantify C and N contaminations in the films due to the higher sensitivity of XPS compared to RBS for these elements. For the XPS analysis, a 400 μm diameter spot was used, and photoelectrons were collected at a take-off angle of 60°. The samples were neutralized during the XPS analysis using an electron flood gun in order to correct for differential or nonuniform charging.

Grazing incidence x-ray diffraction (GI-XRD) was employed to determine the crystalline phases of the HfO_2 thin films. The XRD analysis was performed on a Panalytical X'Pert PRO MRD employing Cu Kα (1.54 Å) radiation with an incidence angle of 0.5° with respect to the substrate plane. Atomic force microscopy (AFM) was used to investigate the surface morphology of the films. The AFM scans were performed in tapping mode with a NT-MDT Solver P47 microscope using a TiN coated Si tip (NSG10/TiN, NT-MDT). Cross-sectional TEM analysis was performed using a JEOL ARM 200 operated at 200 kV. For this, the HfO_2 film was coated with a SiO_x/Pt film stack as a protective layer and subsequently prepared using a standard FIB lift-out TEM sample preparation scheme.

The conformality of HfO_2 ALD process was determined on substrate coupons with high-aspect-ratio (HAR) nanostructures. These HAR nanostructures were created by etching SiO_2 grown by PECVD into the Si wafer. The SiO_2 nanostructures were then coated with a SiNx layer deposited by high-temperature CVD, onto which a SiO_2 thin film was deposited using ALD. The HfO_2 sample was coated with a layer of spin-on epoxy to fill the remaining gaps in the trenches in order to protect the film from curtaining damage during the subsequent lift-out FIB sample preparation.

III. RESULTS AND DISCUSSION

A. ALD growth

The ALD process was characterized by monitoring the GPC by *in situ* SE analysis. The influence of dose steps was investigated by varying the duration of the precursor step, the O_2 plasma step and the purge steps between each half cycle. Figures 1(a)–1(d) show the GPC values obtained at a substrate temperature of 250 °C when varying the HyALD and O_2 plasma exposure steps [Figs. 1(a) and 1(c), respectively], and purge times after the precursor dose and the plasma exposure step [Figs. 1(b) and 1(d), respectively]. The GPC showed a clear saturation behavior for both the precursor and the plasma half cycles resulting in a GPC value of ~1.1 Å/cycle. The Ar purge after the HyALD dose showed a negligible influence on the GPC [Fig. 1(b)]. Also, when no purge step was applied after the precursor dose step, the GPC value did not show a remarkable change. By supplying O_2 during all ALD steps, including the precursor dose, it was verified that the HyALD precursor does not react with the molecular oxygen in the process space investigated, thus excluding the presence of a parasitic CVD component.

The duration of the purge step applied after the plasma step showed however an influence on the growth, in particular a higher GPC was recorded with a decreasing purge time. This is likely caused due to a parasitic CVD growth component due to chemical reactions between the by-products after the plasma step (i.e., H_2O) and the HyALD precursor when low purge times are employed. On the basis of the results in Fig. 1, to guarantee a genuine saturation behavior of precursor and purge steps, a precursor/purge/plasma/purge sequence of 5/2/8/5 s was chosen in this work.

The influence of the substrate temperature on the GPC was also determined. Figure 2(a) shows the thickness evolution of HfO_2 films deposited at substrate stage temperatures ranging between 150 and 400 °C as obtained from *in situ* SE. For all temperatures studied, the films showed a linear growth trend without growth delay as expected for a typical O_2 plasma ALD process. Figure 2(b) shows the

RIGHTSLINK

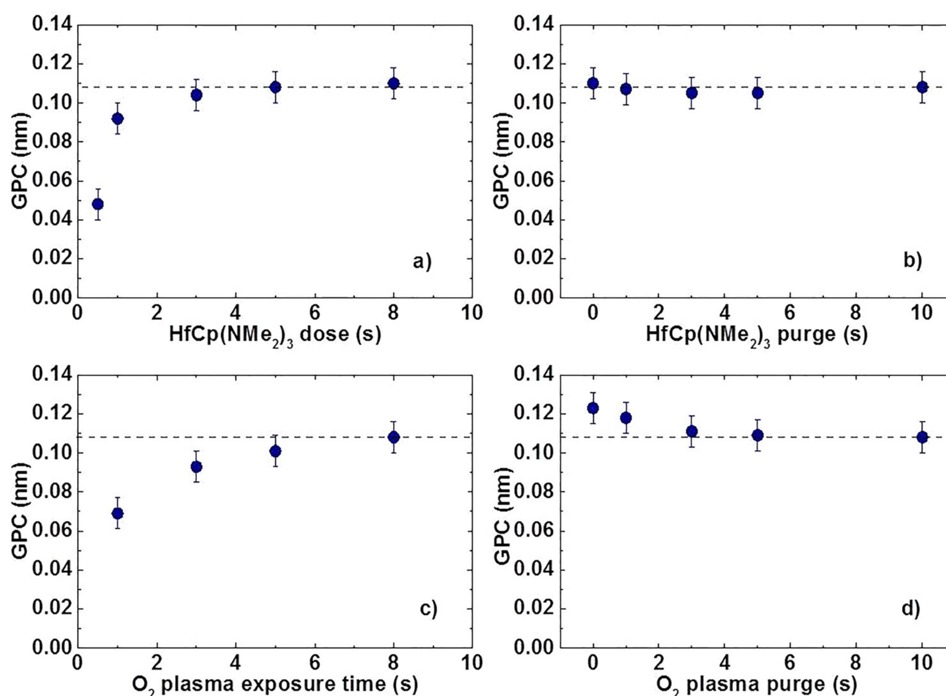

FIG. 1. (Color online) GPC values as a function of (a) HyALD dose; (b) Ar purge time after precursor dose; (c) O_2 plasma exposure; and (d) purge time after the plasma step. The substrate temperature during the process was 250 °C. The dashed lines serve as a guide to the eyes.

GPC values as calculated from Fig. 2(a), corresponding to the studied substrate stage temperatures and the average number of Hf atoms deposited per ALD cycle as determined from RBS measurements. As mentioned above, the high thermal stability of $HfCp(NMe_2)_3$ allows to explore a larger temperature window.[29] The GPC value remains constant at around 1.1 Å/cycle for the whole range of substrate stage temperatures from 150–400 °C signifying the decomposition-free deposition.

The relatively higher GPC value at low temperatures (150–200 °C) can be attributed to a higher incorporation of impurities combined with a lower density of the films for lower deposition temperatures. This hypothesis was confirmed by the elemental composition analysis carried out by XPS and RBS as reported in Table II. The film densities were obtained through the combined RBS and SE analysis, and the stoichiometric ratios for Hf/O were determined from the RBS areal density values for Hf and O, respectively. As reported in Table II, the Hf/O ratio increased with increasing deposition temperature and an excellent stoichiometric value close to ∼0.5 was achieved at 400 °C. The over-stoichiometric films (i.e., oxygen rich) obtained at lower deposition temperatures might be attributed to the formation of hydroxyl impurities. The hydroxyl impurities are directly related to the H content which decreased with the increasing deposition temperature. Furthermore, the N and C levels were below 1 and 2 at. % irrespective of the deposition temperature. The corresponding XPS depth profile spectra for the films deposited at the substrate stage temperature of 400 °C are shown in Fig. 1 of the supplementary material.[35] The low N and C levels obtained are a clear merit, as in earlier work the performance of devices with HfO_2 has clearly shown to degrade with increasing impurity levels.[30,31] Moreover, as will be shown in Sec. III B, the degree of crystallinity increases for higher deposition temperatures.

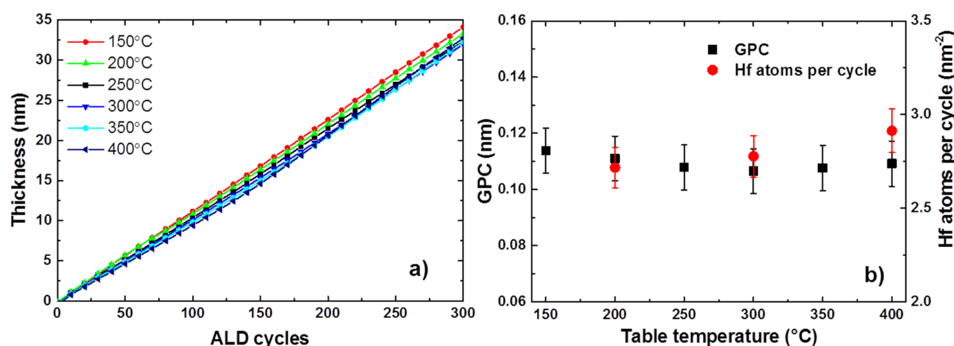

FIG. 2. (Color online) (a) Film thickness as a function of number of ALD cycles with temperature ranging between 150 and 400 °C. The thickness values have been obtained from *in situ* SE. (b) GPC values corresponding to the studied substrate stage temperatures and the average number of Hf atoms deposited per ALD cycle as determined from RBS measurements.

RIGHTSLINK

TABLE II. Elemental composition of HfO_2 films as determined by RBS, ERD and XPS. The typical corresponding errors for Hf/O ratio, density values and H content are mentioned. The Tauc band gap values (E_g) are obtained from SE measurements; a dash (—) means not measured.

Substrate stage temp. (°C)	Hf/O content from RBS	Density from RBS (g/cm^3)	H content from ERD (at. %)	E_g (eV)
150	—	—	—	5.5
200	0.46 ± 0.03	8.7 ± 0.1	3.4 ± 0.2	5.5
250	—	—	—	5.5
300	0.48 ± 0.03	9.0 ± 0.1	1.4 ± 0.1	5.4
350	—	—	—	5.3
400	0.49 ± 0.03	9.3 ± 0.1	0.8 ± 0.1	5.5

As mentioned above, the GPC obtained in this work (1.1 Å/cycle) is considerably higher than the previously reported values in the literature when using $HfCp(NMe_2)_3$ in combination with H_2O (0.23–0.36 Å/cycle) or O_3 (0.75 Å/cycle) as oxidizing agents. This can likely be attributed to the creation of a higher density of reactive surface sites for precursor adsorption owing to the higher reactivity of plasma species.[28] It is also worth mentioning that the usage of plasma species leads to reduction in purge time resulting in shorter cycle times, which impact the overall ALD process throughput.[28] This is corroborated by the fact that $HfCp(NMe_2)_3$ in combination with H_2O requires a long post-H_2O purge time (30 s)[23] as compared to post-O_2 plasma purge time (5 s) in this work which therefore increases the net ALD throughput.

B. Optoelectronic properties and crystallinity

The optical properties of HfO_2 films have been analyzed by *ex situ* SE. Cauchy and B-spline models were used for obtaining the dielectric functions in the fully transparent and absorbing regions, respectively. Figure 3 shows the dielectric function, i.e., the real (ε_1) and imaginary part (ε_2), of ~32 nm HfO_2 films deposited in the temperature range studied. The imaginary part of dielectric function was used to determine the Tauc band gap by plotting $(\varepsilon_2 E^2)^{1/2}$ as a function of photon energy and extrapolating the linear part to zero absorption. The resulting band gap values obtained by this procedure is listed in Table II, and a Tauc plot corresponding to the film deposited at a substrate stage temperature of 400 °C is shown in the supplementary material (Fig. 2). As evident in Fig. 3, the films deposited at higher temperatures have the higher values of ε_1 in the regions with $\varepsilon_2 = 0$. The higher value of ε_1 corresponds to a higher refractive index and is consistent with the elemental analysis: less impurities and a higher density for thin films deposited at high temperatures. Furthermore, the dielectric function of the film deposited at 400 °C shows distinctive sharp features, both in ε_1 and ε_2, compared to the other films. These features can be imputed to a polycrystalline nature of the film leading to sharper electronic transitions. An onset from a smooth dielectric function (<300 °C) to one with sharper features (400 °C) for the film deposited at 350 °C is visible in the inset of Fig. 3.

These findings were corroborated by GI-XRD analysis of the same films as shown in Fig. 4. The GI-XRD spectra of the film deposited at 200 °C showed no distinctive diffraction peaks, and only a broad peak at $2\Theta \sim 32°$ was detected corresponding to amorphous HfO_2. The film deposited at 300 °C also showed a broad peak at $2\Theta \sim 32°$ while a broad diffraction peak with weak intensity, corresponding to the (111) peak of the monoclinic phase, could be detected. This indicates that the HfO_2 thin films studied were mostly amorphous for deposition temperatures up to 300 °C. When increasing the deposition temperature to 350 °C, a clear transition in the GI-XRD spectra could be seen. Diffraction peaks corresponding to the monoclinic, tetragonal, and cubic HfO_2 phases were detected, indicating a higher degree of crystallinity as compared to lower deposition temperatures of 200 and 300 °C. By further increasing the substrate stage temperature to 400 °C, peaks having higher intensity were measured indicating a higher degree of crystallinity. The monoclinic phase appeared to be dominant at this deposition temperature.

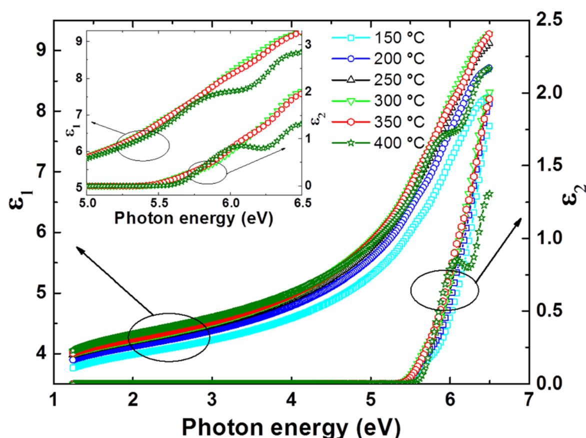

FIG. 3. (Color online) Real (ε_1) and imaginary (ε_2) part of the dielectric function as a function of photon energy measured by *ex situ* SE. The sharp features at a growth temperature of 400 °C indicate the polycrystalline structure of the film. The transition from smooth to sharp dielectric function for films grown at 400 °C can be observed in the inset.

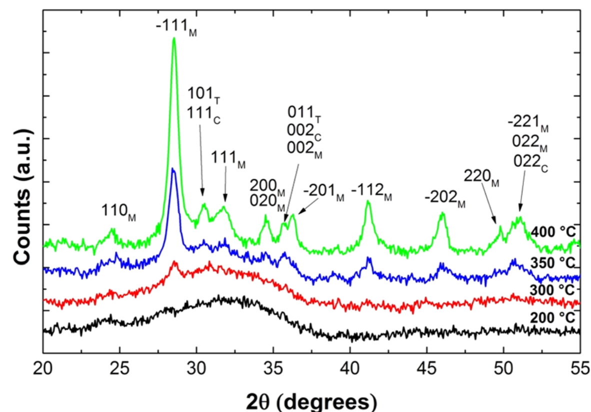

FIG. 4. (Color online) GI-XRD diffractogram for 32 nm thick HfO_2 films prepared by ALD. The substrate stage temperatures during deposition are indicated by the labels. The subscripts M, T, and C at indices denote monoclinic, tetragonal, and cubic phases, respectively. The spectra show a clear temperature dependence of the HfO_2 film crystallinity with a transition from amorphous to polycrystalline films embarking at a temperature of 300 °C.

RIGHTSLINK

The GI-XRD patterns obtained in this work are remarkably similar to the ones reported by Niinistö *et al.*,[24] for the HfO_2 ALD process employing the same precursor, $HfCp(NMe_2)_3$, and O_3 as the oxidizing agent. In their work, Niinistö *et al.* showed a similar temperature dependence of the HfO_2 film crystallinity with a clear transition from amorphous to crystalline films at a deposition temperature of 300 °C. The difference in temperature between this work and the one reported by Niinistö *et al.* at which this transition could be observed is imputed to a ∼20%–25% difference between the set stage temperature value and the actual substrate temperature for the reactor employed in this work.[32] It can be concluded that the crystallization temperature of HfO_2 films is rather independent of the oxygen source used in combination with $HfCp(NMe_2)_3$ during the ALD process. However, the usage of a plasma-assisted ALD process may open the possibility for tuning of the crystalline phase by ion bombardment by employing substrate biasing during processing,[33] which is the object of further investigation.

Figure 5 shows a cross-sectional TEM image of a ∼32 nm HfO_2 film deposited at 400 °C on H-terminated Si substrate. The full Si/HfO_2 (32 nm)/SiO_x (∼100 nm)/Pt stack is shown in Fig. 5(a). The HfO_2 film shows a sharp interface with the underlying Si substrate, while an interface with higher roughness was formed with the overlying protective SiO_x layer due to the crystalline HfO_2 grains.

A close inspection of Fig. 5(b) reveals the presence of an amorphous SiO_2 layer at the Si/HfO_2 interface. The amorphous nature of the Si substrate is imputed to damage caused by the focused ion beam used during sample preparation. The TEM image shows that the HfO_2 film is fully crystalline which is in line with the GI-XRD analysis. Furthermore, individual HfO_2 grains can be identified [Fig. 5(b)] with an average lateral grain size of ∼20–30 nm.

C. Surface morphology

The AFM scans over an area of $500 \times 500\,nm^2$ for the ∼32 nm thick HfO_2 films (300 ALD cycles) deposited at 200, 300, 350, and 400 °C are depicted in Figs. 6(a), 6(b), 6(c), and 6(d), respectively. The root-mean-square (RMS) roughness values obtained from $2 \times 2\,\mu m^2$ AFM scans of the same samples are indicated in Figs. 6(a)–6(d). For the film deposited at 200 °C, a very smooth surface (RMS = 1.29 nm) with very few randomly distributed singular features was obtained [see Fig. 6(a)]. The higher substrate stage temperature of 300 and 350 °C yielded an increase in density and size of these singular features as depicted in Figs. 6(b) and 6(c). The RMS roughness values also showed an increment with increasing deposition temperature from 200 to 350 °C. AFM scans of the HfO_2 sample deposited at 400 °C revealed a slightly different film morphology with a decreased RMS roughness value compared to the film deposited at 350 °C [Fig. 6(d)]. On the basis of the obtained morphology, it can be argued that the singular features observed might be associated with the increasing degree of crystallinity with the increase in deposition temperature from 200 to 350 °C resulting in a transition from amorphous to polycrystalline films as shown before in Figs. 3 and 4 corresponding to the SE and GI-XRD analyses. Furthermore, the lower RMS roughness value obtained at 400 °C might be attributed to the full crystallization obtained already during the deposition process leading to a laterally homogeneous and smooth HfO_2 thin film, which is also supported by TEM image (Fig. 5).

This effect was also confirmed for thicker films as depicted in Figs. 6(e) and 6(f) with $500 \times 500\,nm^2$ AFM scans of ∼80 nm HfO_2 films deposited at 250 and 400 °C, respectively. The RMS roughness values of these two films are also indicated in Figs. 6(e) and 6(f). The increase in RMS as a function of layer thickness of the samples grown at 400 °C can be explained by grain coarsening, i.e., increase in (lateral) grain size as a function of film height. The film deposited at 250 °C shows higher surface roughness compared to the one deposited at 400 °C, most likely because of coalescence of individual crystalline grains at 400 °C in the top part of the layer.

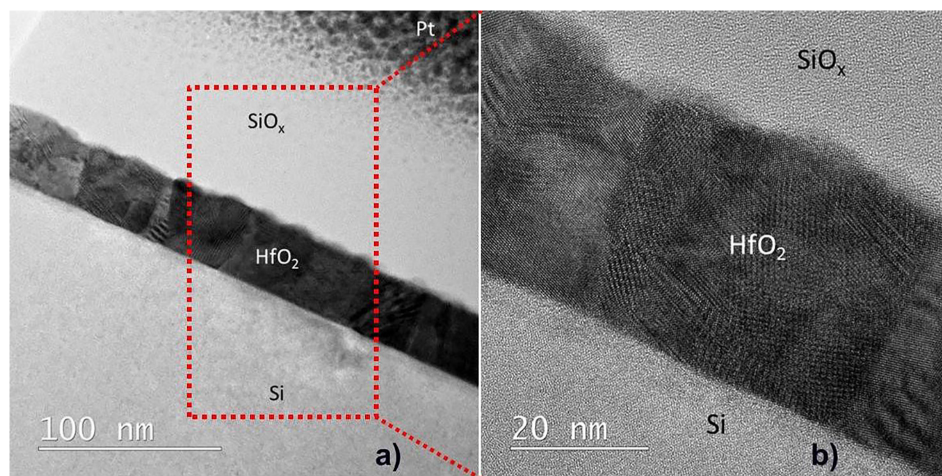

Fig. 5. (Color online) (a) Cross-sectional TEM image of a ∼32 nm HfO_2 film deposited at 400 °C on a H-terminated Si substrate. The Si/HfO_2 (32 nm)/SiOx (∼100 nm) stack demonstrating a sharp interface between HfO_2 and underlying Si has been highlighted within a square. (b) A close up of the cross-sectional TEM image clearly showing the individual crystalline grains of HfO_2 and an amorphous SiO_2 layer at the Si-HfO_2 interface.

RIGHTSLINK

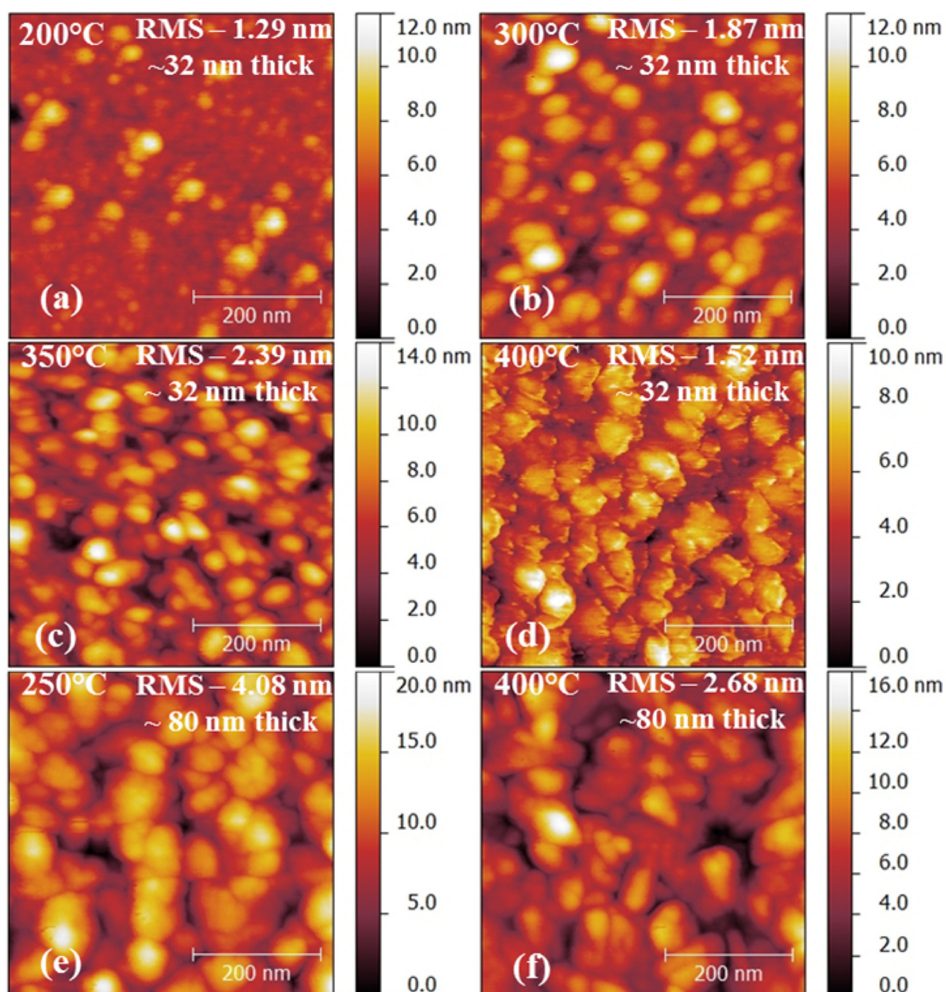

FIG. 6. (Color online) AFM scans with a scan area of 500 × 500 nm of the ~32 nm HfO_2 films (300 ALD cycles) deposited at (a) 200 °C, (b) 300 °C, (c) 350 °C, and (d) 400 °C. An increase in amount of the crystallites can be detected from 200 to 400 °C indicating enhanced crystallinity with increase in substrate stage temperature. Similar AFM scans of thicker ~80 nm HfO_2 (750 ALD cycles) films deposited at (e) 250 °C and (f) 400 °C show higher roughness.

D. Conformality

The conformality of the above HfO_2 ALD process was determined by depositing a ~20 nm thick HfO_2 film over HAR nanostructures with varying aspect ratio (0.6–9) at a deposition temperature of 250 °C. Figure 7 shows a cross-sectional TEM image of the HAR trench structures conformally covered with the HfO_2 film. It should be noted that the deposition conditions for this purpose were kept the same as implemented for the planar Si substrates. A comparison of the HfO_2 film thickness on the side walls and planar areas of the nanostructures shows that the HfO_2 films had a conformality of 79% and 72.2% for aspect ratios of 3 and 7.3, respectively. A further optimization of the precursor

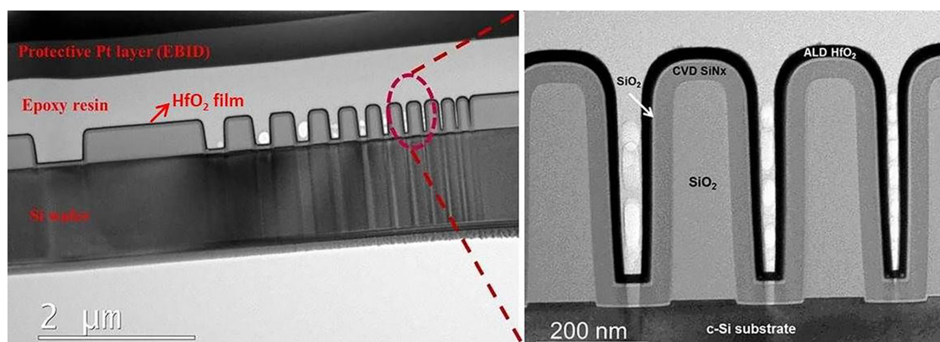

FIG. 7. (Color online) (Left) Cross-sectional transmission electron microscopy image of a conformal HfO_2 layer deposited on high aspect ratio nanostructures by ALD at 250 °C using $HfCp(NMe_2)_3$ and O_2 plasma. (Right) A close up of trench structures with varying aspect ratios shows the conformal HfO_2 thin film.

RIGHTSLINK

dose and plasma conditions is required to exclude the recombination- or diffusion-limited regimes being the limiting factors for the step coverage.[34]

IV. SUMMARY AND CONCLUSIONS

In this study, a plasma enhanced atomic layer deposition process for the deposition of HfO_2 thin films using a hafnium precursor [$HfCp(NMe_2)_3$] comprising cyclopentadienyl-alkylamido ligands in combination with O_2 plasma has been evaluated. The growth characteristics clearly show the high thermal stability and high growth rate of the used precursor combined with O_2 plasma yielding a high GPC value of ~1.1 Å/cycle over a wide ALD temperature range of 150–400 °C. High purity HfO_2 thin films were obtained even at fairly low deposition temperatures with carbon and hydrogen residual impurity contents below 2 and 3.5 at. %, respectively, for the whole range of substrate stage temperature investigated. A high substrate stage temperature of 400 °C resulted in fully crystalline, predominantly monoclinic as-deposited HfO_2 thin films with a high refractive index and a smooth surface. It was also found that the $HfCp(NMe_2)_3$ in combination with O_2 plasma requires shorter ALD cycle time relatively as compared to the ALD process using H_2O as oxidizing agent and therefore the plasma-enhanced ALD process offers a promising and viable method complementary to the thermal ALD process for producing high quality HfO_2 thin films.

ACKNOWLEDGMENTS

The authors gratefully acknowledge Cristian van Helvoirt for technical assistance, Harm Knoops, Vincent Vandalon for fruitful discussion and Lam Research for providing substrates with HAR trench structures. The authors would like to acknowledge AirLiquide for providing the Hf precursor. They would also like to acknowledge W. Keuning and B. Barcones for the FIB sample preparation and Solliance Solar Research for funding the TEM facility. One of the authors (W. M. M. Kessels) would like to acknowledge "Gravitation project" for making this research work possible. This work is part of the Research Centre for Integrated Nanophotonics (NWO-578467 024.002.033), which is partly financed by the Netherlands Organization for Scientific Research (NWO).

[1]M. Houssa, L. Pantisano, L. Å. Ragnarsson, R. Degraeve, T. Schram, G. Pourtois, S. De Gendt, G. Groeseneken, and M. M. Heyns, Mater. Sci. Eng., R **51**, 37 (2006).
[2]E. P. Gusev, C. Cabral, Jr., M. Copel, C. D'Emic, and M. Gribelyuk, Microelectron. Eng. **69**, 145 (2003).
[3]M. Cho, H. B. Park, J. Park, S. W. Lee, C. S. Hwang, G. H. Jang, and J. Jeong, Appl. Phys. Lett. **83**, 5503 (2003).
[4]G. D. Wilk, R. M. Wallace, and J. M. Anthony, J. Appl. Phys. **89**, 5243 (2001).
[5]M. Gutowski, J. E. Jaffe, C.-L. Liu, M. Stoker, R. I. Hegde, R. S. Rai, and P. J. Tobin, Appl. Phys. Lett. **80**, 1897 (2002).
[6]B. Radisavljevic, A. Radenovic, and J. Brivio, Nat. Nanotechnol. **6**, 147 (2011).
[7]V. Djara *et al.*, Microelectron. Eng. **147**, 231 (2015).
[8]M. Berdova *et al.*, Appl. Surf. Sci. **368**, 470 (2016).
[9]L. Zhang, H. Nakanotani, K. Yoshida, and C. Adachi, Org. Electron. **15**, 1815 (2014).
[10]W.-J. Yoon and P. R. Berger, Org. Electron. **11**, 1719 (2010).
[11]S. M. George, Chem. Rev. **110**, 111 (2010).
[12]M. Ritala, M. Leskelä, L. Niinistö, T. Prohaska, G. Friedbacher, and M. Grasserbauer, Thin Solid Films **250**, 72 (1994).
[13]K. Kukli, M. Ritala, T. Sajavaara, J. Keinonen, and M. Leskelä, Thin Solid Films **416**, 72 (2002).
[14]H. B. Park *et al.*, J. Appl. Phys. **94**, 3641 (2003).
[15]J. J. Ganem, I. Trimaille, I. C. Vickridge, D. Blin, and F. Martin, Nucl. Instrum. Methods Phys. Res., Sect. B **219–220**, 856 (2004).
[16]J. Niinistö, K. Kukli, M. Heikkilä, M. Ritala, and M. Leskelä, Adv. Eng. Mater. **11**, 223 (2009).
[17]K. Kukli, M. Ritala, T. Sajavaara, J. Keinonen, and M. Leskelä, Chem. Vap. Deposition **8**, 199 (2002).
[18]D. M. Hausmann, E. Kim, J. Becker, and R. G. Gordon, Chem. Mater. **14**, 4350 (2002).
[19]Y. Senzaki, S. Park, and H. Chatham, J. Vac. Sci. Technol., A **22**, 1175 (2004).
[20]S. B. S. Heil, V. J. L. Hemmen, and C. J. Hodson, J. Vac. Sci. Technol., A **25**, 1357 (2007).
[21]J. Niinistö, M. Putkonen, L. Niinistö, S. L. Stoll, K. Kukli, T. Sajavaara, M. Ritala, and M. Leskelä, J. Mater. Chem. **15**, 2271 (2005).
[22]J. Niinistö, M. Putkonen, L. Niinistö, and F. Song, Chem. Mater. **19**, 3319 (2007).
[23]S. Consiglio, R. D. Clark, and G. Nakamura, J. Vac. Sci. Technol., A **30**, 01A119 (2012).
[24]J. Niinistö, M. Mäntymäki, K. Kukli, L. Costelle, E. Puukilainen, M. Ritala, and M. Leskelä, J. Cryst. Growth **312**, 245 (2010).
[25]E. Granneman, P. Fischer, D. Pierreux, H. Terhorst, and P. Zagwijn, Surf. Coat. Technol. **201**, 8899 (2007).
[26]L. Aarik, H. Alles, A. Aidla, T. Kahro, K. Kukli, and J. Niinistö, Thin Solid Films **565**, 37 (2014).
[27]A. Matin, A. B. Robert, M. P. Robert, and D. Madan, Nanotechnology **26**, 115202 (2015).
[28]H. B. Profijt, S. E. Potts, and M. C. M. de Sanden, J. Vac. Sci. Technol., A **29**, 050801 (2011).
[29]N. Blasco, Air Liquide, private communication (21 August 2013).
[30]M. Choi, J. L. Lyons, A. Janotti, and C. G. Van de Walle, Appl. Phys. Lett. **102**, 142902 (2013).
[31]G. Niu, H.-D. Kim, R. Roelofs, E. Perez, M. A. Schubert, P. Zaumseil, I. Costina, and C. Wenger, Sci. Rep. **6**, 28155 (2016).
[32]V. Longo, N. Leick, F. Roozeboom, and W. M. M. Kessels, ECS J. Solid State Sci. Technol. **2**, N15 (2012).
[33]H. B. Profijt, M. C. M. van de Sanden, and W. M. M. Kessels, Electrochem. Solid-State Lett. **15**, G1 (2011).
[34]H. C. M. Knoops, E. Langereis, M. C. M. van de Sanden, and W. M. M. Kessels, J. Electrochem. Soc. **157**, G241 (2010).
[35]See supplementary material at http://dx.doi.org/10.1116/1.4972210 for XPS depth profile plot and Tauc Plot for bandgap value extraction.

RIGHTSLINK